Optical and Quantum Electronics (2019) 51:321
https://doi.org/10.1007/s11082-019-2037-z

A 7.4 kHz, 20-bit image encoder with a CMOS linear image sensor

Yusong Mu[1] · Jiaqi Jiang[1] · Ning Ding[1] · Qiliang Ni[2] · Yuchun Chang[1]

Received: 9 June 2019 / Accepted: 14 September 2019

Abstract
This paper presents a unique CMOS linear image sensor for reading the pseudo-random code on the slit disc, focusing on the two aspects of low noise and readout rate. Each pixel is equipped with an exclusive integral readout circuit, and the shape of the pixel also matches the slit disc, making the output signal consistent by up to 99%. After subdivision, the absolute angle data can be captured with an angular resolution of 16 bits and a maximum speed of 7.4 kHz. In addition, decoding and subdivision methods are suitable for high-speed, inexpensive encoder systems.

Keywords Integrated optics · Sensors · Metrological instrumentation · Photoelectric device

1 Introduction

The traditional rotational displacement measurement technology is limited in terms of resolution and precision, due to the mechanical adjustment process and the engraving technology of the slit disc, etc. (Mancini et al. 1997; Pertiu 1987; Tomlinson 1987). In recent years, many researchers have explored various encoders in regards to their practical application based on image processing technology (Luo et al. 2016; Qin et al. 2016; Sobieranski et al. 2015). Compared with the traditional method, the image encoder has the advantages in the following two aspects: firstly, it is simplified in the adjustment process, from the eccentricity adjustment of the double metering grating to the eccentric adjustment of the slit disc; Secondly, the resolution of the rotational displacement measurement is effectively improved by developing the detector performance without changing the size of the slit disc. Therefore, the key technology of image encoder is that the sub-pixel precision measurement of the image depicted by the code channel, and it will continue to improve with the development of modern digital image processing technology (Kao et al. 2010; Feng et al. 2013; Jin et al. 2014).

✉ Yuchun Chang
changyc@jlu.edu.cn

[1] State Key Laboratory on Integrated Optoelectronics, College of Electronic Science and Engineering, Jilin University, Changchun 130012, China

[2] Changchun Institute of Optics, Fine Mechanics and Physics, Chinese Academy of Sciences, Changchun 130033, China

Published online: 21 September 2019

Since the twenty-first century, we have seen remarkable developments in photoelectric encoder with area-array image sensor as photoelectric detector. The most iconic of these is NASA's first proposed method of reading absolute code and subdivision with an area CCD sensor, which features resolution up to 0.01″ in a lab environment (Leviton and Frey 2003). In another landmark study, the Hamamatsu Corporation in Japan created an absolute shaft encoder based on an area CMOS sensor that can reach 14 bit resolution and 3.2 kHz frame rate (Sugiyama et al. 2008). Lleida University in Spain used the principle of CMOS image sensor and optical mice to obtain image information and a microprocessor for angle measurement, effectually developing a high-resolution systems that is very low in cost (Tresanchez et al. 2010). Research institutes in Korea had developed an absolute angle measurement method that used a 10 bit or 13 bit phase-encoded binary graduated disk (PE-BGD) to achieve maximum angular measurement errors of 25″ and 4″ in frequency response of 500 Hz (Kim et al. 2016). The above research shows that the image encoder has excellent performance in the resolution of angle measurement, but ignores the important index of readout speed.

In 2017, Changchun Institute of Optical, Fine Mechanics and Physics (CIOMP), Chinese Academy of Sciences proposed a scheme with the pseudo-random code on the slit disc and the CCD linear-array sensor as a photoelectric detector (Yu et al. 2017). This scheme made full use of the space of the slit disc, could accomplish the high resolution encoding on the small size disc, and improved the frequency response (Yuan et al. 2019). The problem of matching fan-shaped disc and linear-array image sensor make most pixels work under unsaturated state. As a result, the sensor is affected by light noise and fixed pattern noise, which did not achieve measurement accuracy.

A few notable conclusions can be drawn based on review of the literature. The key problem in the field of image encoder is how to improve the reading speed of image sensor to meet the speed of encoder, and to ensure the quality of image sensor reading signal. In this context, a unique linear-array image sensor is designed, and its pixel size and angle fully match the slit disc, which implementations the readout of the analog signal with low noise and high consistency. After subdivision calculation, we propose the image encoder system which is capable of 7.4 kHz continuous detection with 16 bit resolution.

This paper is organized as follows. In Sect. 2 the profile sensor, which is designed for position detection, is explained. Section 3 describes the overall encoder system and discusses its performance. Section 4 provides a brief summary and conclusion.

2 Design of detector

2.1 Concept

The sensor is a CMOS linear image sensor specially designed for high-speed position detection of weak light. We use a LED light source to irradiate the slit dick, and light passes the slit disc onto the sensor as shown in Fig. 1. The sensor is designed to capture light and convert the optical signal into an analog signal output. The linear-array is listed as 120 independent pixels to complete the acquisition of optical signals, each pixel area of $25 \times 610\ \mu m^2$. The pseudo-random code disc has 1024 indexes located at a constant angular pitch of 0.35°, and each index consists of a 10 bit code on the same circular track. The size of each hole is $150.9 \times 610\ \mu m^2$, and it happens to have the same photosensitive area as six pixels.

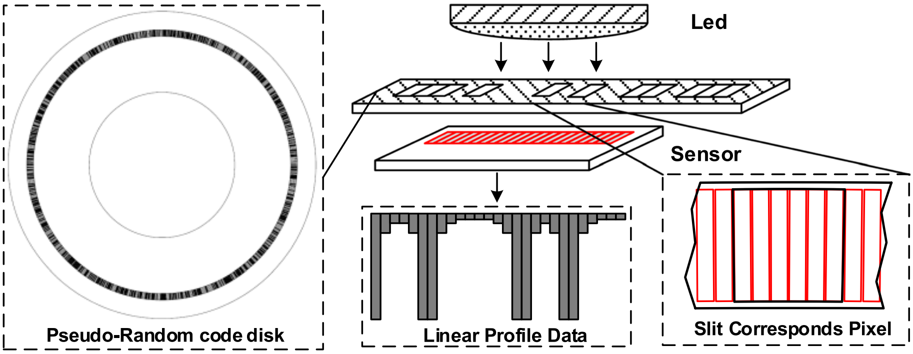

Fig. 1 Principle of reading pseudo-random code

The complete architecture of the sensor designed in this paper is shown in Fig. 2. The readout circuit of array arrangement can ensure that the output signal has a high signal-to-noise ratio. Each pixel is equipped with an exclusive integral readout circuit which layout is designed to be 25 μm wide in a narrow shape, so large compensating capacitors cannot be used. In other respects, the narrow pixel shape makes it difficult for the readout circuit to achieve the output of the analog signal that can be quantified by 12 bit. Therefore, we designed a level two op-amplifier (with dual-end input single-ended output) to ensure that the DC gain of amplifier is above 80 dB. Compared with the traditional single-stage switching capacitor amplifier, the structure of this paper requires less capacitance and faster sampling speed. Other functional circuits include integral sampling capacitors, line selector switches, and output level Buffer.

3 Circuit design

In this paper, the structure of the op-amplifier is shown in Fig. 3, which mainly includes the first stage input amplifier circuit, the second stage amplifier circuit and the bias circuit. The main op-amplifier consists of M1–M5, which selects the structure of the dual-end input single-end output, which can effectively suppress the common-mode noise

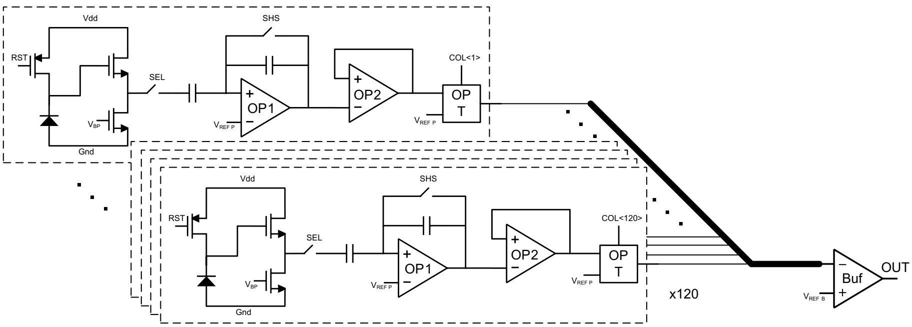

Fig. 2 Configuration of sensor

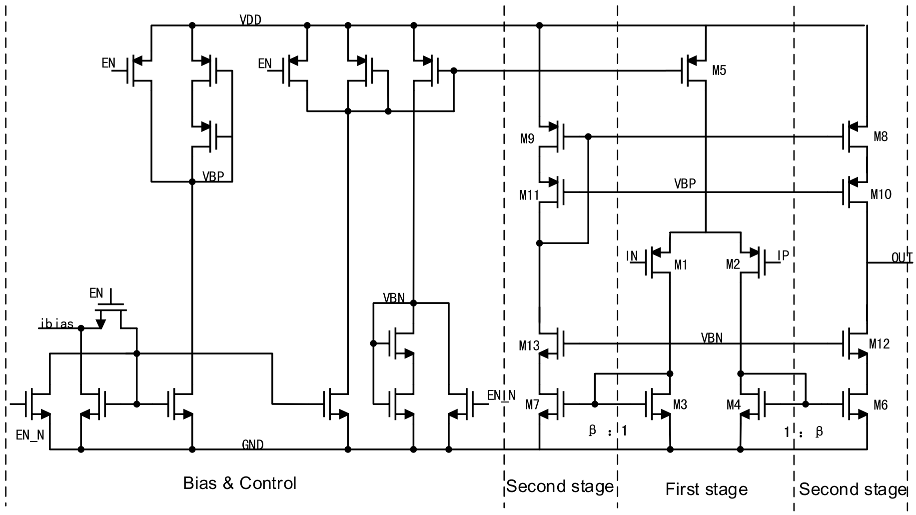

Fig. 3 Op-amplifier circuit

and provide a large output swing. The output-level amplifier consists of M6–M13, which increases the pendulum rate of the circuit (slew rate) by increasing the M10–M13. The rest of the parts are bias and enabling circuits.

The following is a calculation of the specific parameters of the transistor in the op-up, which is Transconductance to:

$$G_M \approx \beta g_{m1}^2 \tag{1.1}$$

The beta represents the ratio of M7 to M3, and the operational amplifier output is:

$$R_{out} \approx r_{o6} g_{m12} r_{o12} \tag{1.2}$$

The intrinsic gain of the transistor can be calculated by setting the gain beyond 80 dB. Therefore, we set L to 1 to ensure that the intrinsic gain of the transistor is greater than 40 dB.

$$A_v \approx \beta g_{m1}^2 r_{o6} g_{m12} r_{o12} \tag{1.3}$$

The dominant pole of the operational amplifier is the output node, and the GBW (gain-bandwidth product) of the operational amplifier is

$$GBW = \frac{\beta g_{m1}}{C_L} \tag{1.4}$$

The load capacitance is 20 pF and the GBW is greater than 7 MHz, the g_{m1} of input pair tube value is 12.6×10^{-6} S. Where $g_{m1} = 2i_d/v_{ov}$, we set the v_{ov} as a typical value of 0.15 V, can be calculated with i_d of 1.3 μA. We can calculate to get W/L by the gm/id curve obtained of simulation. Entering the branch current of the tube to 1.3 μA, we know that the value of each current is calculated, and the W/L value of each transistor is obtained. Therefore, the maximum input range of the operational amplifier is $vdd - v_{ov4} - v_{TH1}$, with a minimum value of $v_{ov5} + v_{TH5} - v_{ov1}$, and the maximum output range of the operational amplifier is $vdd - 2v_{ov}$, with a minimum value of $2v_{ov}$.

The simulation model is established using the above formula, and the open-loop AC simulation of the operational amplifier is obtained with the release gain of 94.8 dB. We get the GBW for 7 MHz, and the output common-model circumference for 600 mV–4.5 V. Then the closed-loop AC simulation of the operational amplifier is concluded that the gain is 91.8 dB. So the GBW is 5 MHz, and the phase margin is 60.6°.

3.1 Circuit noise

The readout unit designed in this paper is a typical direct injection CMOS circuit structure, which has the characteristics of small layout area and low power consumption. The main noise of this circuit is the reset noise of the switch and the thermal noise of the amplifier, which is considered separately because the two noise sources are non-related (Schreier and Silva 2005; Johnson and Lomheim 2009; Vermeiren et al. 2009; Song et al. 2016) (Fig. 4).

Firstly, we assume that the amplifier output impedance is high enough. Thus, the power spectral density (PSD) of switching thermal noise can be approximated as the following formula.

$$S_n(f)=\frac{4kT}{R_{on}} \tag{1.5}$$

where k is the Boltzmann constant and T is the thermodynamic temperature. R_{on} is the on-resistance of the MOS switch, usually $R_{on} \ll 1/g_m$. So the expression that gets the switching thermal noise is shown below.

$$\overline{q_n^2} = \int_0^\infty S_n(f)\left|H_n(S)\right|^2 df = kT\left(C_f + \frac{C_f C_S}{C_f + C_L + C_S}\right) \tag{1.6}$$

Similarly, we analyze the amplifier thermal noise to produce the PSD as shown in the following expression.

$$S_a(f) = 4kT\gamma g_m \alpha \tag{1.7}$$

Referring to the Tapeout process, γ is between 1 and 1.5. α represents the contribution of the load to noise. The expression of amplifier thermal noise is shown below.

$$\overline{q_a^2} = \int_0^\infty S_a(f)\left|H_a(S)\right|^2 df = kT\gamma\alpha\left(\frac{C_S}{C_f + C_L + C_S}\right) \tag{1.8}$$

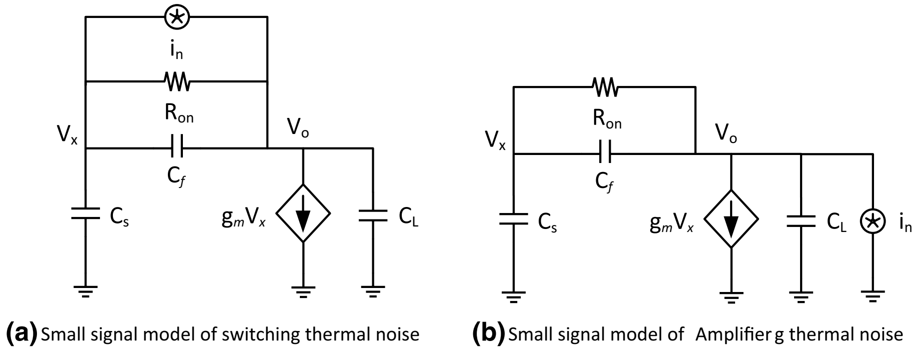

Fig. 4 Small signal model analysis

The total readout noise can be expressed as

$$\sigma = \frac{1}{\mathrm{q}}\sqrt{\mathrm{k}T\left(C_f + \frac{C_S + C_f}{C_f + C_L + C_S} + \frac{\gamma\alpha C_S^2}{C_f + C_L + C_S}\right)} \tag{1.9}$$

The capacitance in this design in total 109 fF, which is brought into the formula and the total noise of the read-out circuit is below 100e-magnitude. The size of the detection is large, and the dark current is 15 pA according to the dark current value of 0.75 fA/μm^2 per unit area. The detector's dark current far exceeds the noise of the circuit, so the key of chip design is to ensure the uniformity of the readout unit.

3.2 Implementation

The sensor was fabricated using the 0.35 μm, 1-poly, 3-metal technology. It is a passive pixel sensor and its photodiode is realized with a junction between a p-diffusion and an n-well. Figure 5 shows a photograph of the chip die, occupying 3.5 mm × 1.8 mm. On one side of the chip, there is a 120-pixel fan-array. The pixel pitch is 25 μm, and therefore, the size of the active area is approximately 3.3 mm × 1 mm. On the other side of the chip, there are 120 separate readout circuit, with an area of 25 μm × 610 μm for each group of read-out circuits, including 3T-pixels, two-stage operational amplifier, capacitance, and trigger switches.

Table 1 is shown that the main characteristics of the sensor.

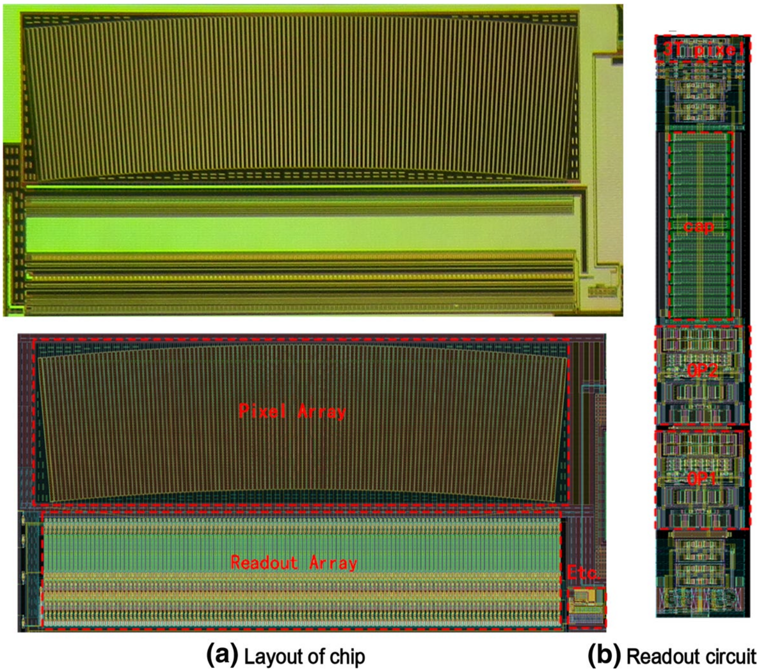

Fig. 5 Layout and photograph of chip

Table 1 Main characteristics of chip

Technology	0.35 µm, 1P3M, CMOS
Die size	3.5×1.8 mm^2
Pixel pitch	20 µm
Array size	120 pixel
Output	1 ports (serial)
Frame rate	7400 frame/s
Supply voltage	3.3 V
Power dissipation	16 mW@3700 frame/s
Pixel uniformity	99%

4 Experiments and subdivision

4.1 Image encode system

The overall measurement system mainly includes: slit-disc, detector to be measured, uniform light source, ADC module, FPGA timing control, logic analyzer, power supply and computer, etc. The sensor and acquisition devices was attached to FPGA which provided them with timing control. Output signal from the sensor was transmitted to the analog-to-digital converter (the AD9226-type ADC), which converted analog signals to 12 bit digital signals at 4 MHz frequencies. Output data from ADC was collected by the logic analyzer and sent to the computer, which calculated the accurate location of the slit disc.

Figure 6 shows the indicator of photo response non-uniformity (PRNU) of the sensor's pixels, the results of which describe the high consistency between the sensor pixels. The

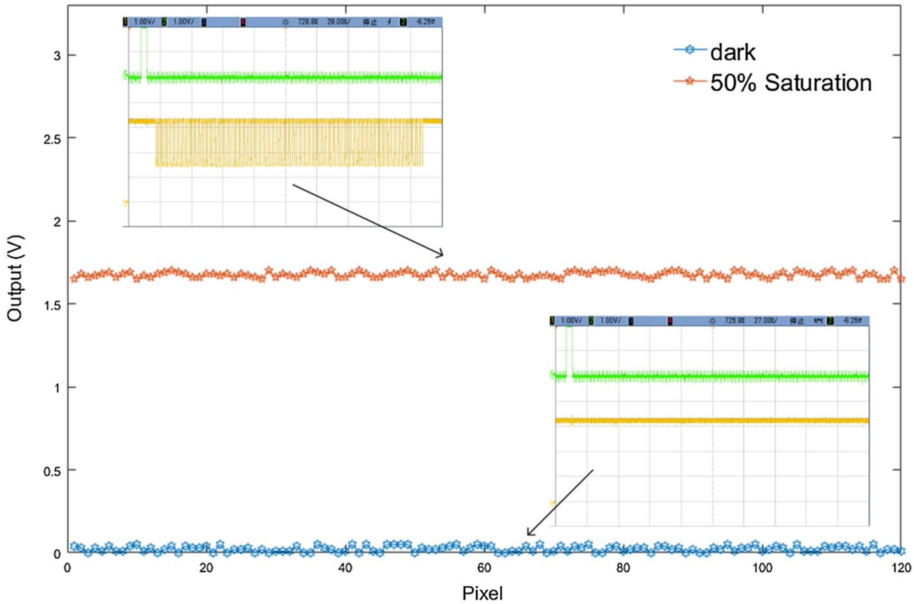

Fig. 6 Photo response non-uniformity data

PRNU values of the EMVA 1288 standard are based on spatial standard deviations (European Machine Vision Association 2012):

$$PRNU = \frac{\sqrt{s_{y.50}^2 - s_{y.dark}^2}}{\mu_{y.50} - \mu_{y.dark}} \tag{1.10}$$

The type μ is the average which is performed over all pixels of the sensor in the dark and 50% saturation output. Likewise, the spatial variances s^2 of dark and 50% saturation are denoted. The data in Fig. 6 is calculated to obtain the PRNU of 1.02%.

Figure 7 shows a photograph of our measurement system. The sensor is placed at the below of the slit disc, and a LED was located at the opposite side. We find that in the smallest transmittance area of the slit disc, the four pixels located in the middle part are fully visible, and two pixels at the edge are partially obscured. Such a matching relationship makes the vast majority of pixels in an ideal saturation state, and a few pixels at the edge of the transmittance zone are in an unstable condition. The case of index code shown in the figure is "11001101000000100101".

Figure 8 shows the analog signal for sensor output display with oscilloscope. The details of the signal were shown that the pixels reached saturation or cut-off, except for a few pixels at the bright and dark edges of the slit disc. The pixel-array was designed to correspond to a code of six pixels. The sensor designed according to the above effectively avoids the diffraction of light and the influence of pixel fixed noise, by making as many pixels work as possible in an ideal state.

Figure 8b shows a gray-scale value which is restored by the data of the logic analyzer. In this figure, the gray-scale value is an index code of slit disc. The six peaks represent holes of the index. We can get the value of 1–1024 range to ensure the stability and accuracy of the system by using the ADC above 10 bit ENOB for linear conversion.

Figure 8c shows the index number code is "11001101000000100101", which is the result of the gray-scale value being processed by binarization. In addition, the result indicates the

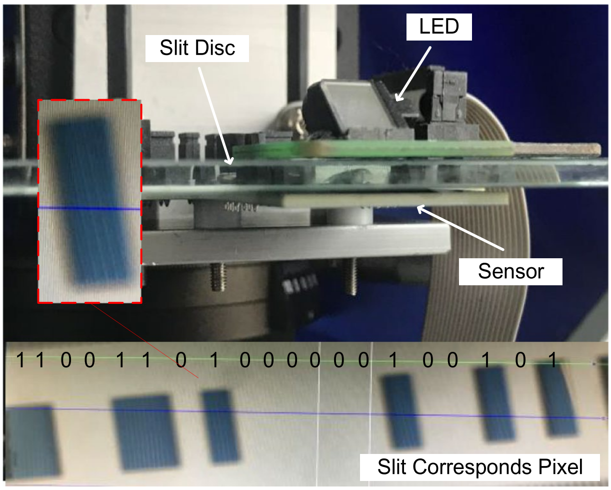

Fig. 7 Details of the slit corresponds pixel

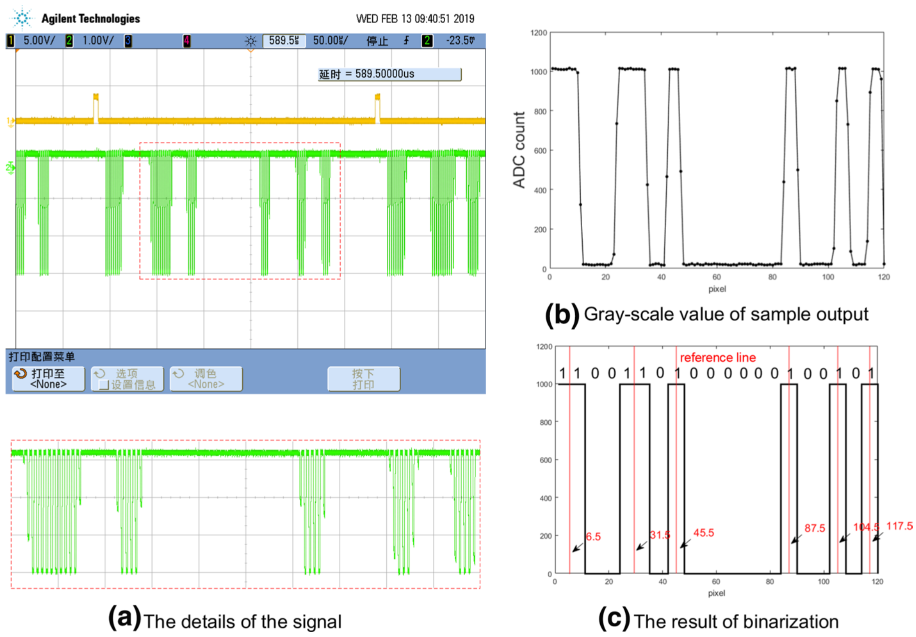

Fig. 8 Output analog signal and data

position of the index. The position of the index also accurately reflects the angle of the slit disc.

4.2 Subdivision

The sub-pixel subdivision algorithm described here was developed based on the "centroid algorithm". It subdivides the angular displacement between consecutive codes by recognizing reference lines. The traditional gray-scale centroid algorithm can be calculated as follows:

$$Y = \sum_{i=1}^{n} P_i G_i \Big/ \sum_{i=1}^{n} P_i \tag{1.11}$$

The P_i is the gray-scale value of i pixel point, the G_i is the position value of the pixel point, and the n is the window size (n values is 8). The centroid calculation of all the photosensitive positions representing "1" in Fig. 8b. Compare the deviation value of the centroid and the reference line of each photosensitive position, that is, the sub-pixel positioning.

The six deviation values of the gray-scale centroid positions and detection lines shown in Table 2. Through calculating the average of these six centroid positions, we can determine the deviation of the index code with the following formula (Yuan et al. 2019):

$$X_E = \frac{1}{N} \sum_{i=1}^{n} Y_i \tag{1.12}$$

Table 2 The value of centroid and deviation

Centroid (Y)	5.623	30.644	44.613	86.630	103.615	116.774
Detection	6.5	31.5	45.5	87.5	104.5	117.5
Deviation	−0.98	−0.96	−0.89	−0.87	−0.83	−0.78

In Eq. 1.13, the X_E is the deviation value of the index code. The Y_i is the value of each centroid. The n is the number of centroid in the window. It is calculated that the deviation of slit disc to the left is approximately 0.885 pixel with sensor as a reference. The spatial variances result is 4.85×10^{-2} by using the data in Table 2. In this paper, we can achieve a 120 times-fold subdivision of the index code, which is designed six pixels corresponded to an index code.

Subdivision of the obtained value β as follows:

$$\beta = X_E \cdot \frac{25}{150.9} \cdot 2^m \tag{1.13}$$

In Eq. 1.14, the pixel pitch is 25 μm, the distance is 150.9 μm, and the m is the number of bits subdivided. We take m to 10 to meet the requirements of accuracy in this paper. Combined with the 10 bit PRBS-value obtained in Sect. 3.1, the resolution of 20 bit angle measurement is realized.

4.3 Measurement

The experiment described above showed that the code number is essential for determining the rotation angle. The precise angular position of the slit disc was calculated with the following equation:

$$Angle\,(^\circ) = ICN \cdot 0.3615 + X_E \cdot \frac{25}{150.9} \tag{1.14}$$

In the Eq. 1.14, the ICN is the value of index codes decoding, and 0.3515 is the angle value represented by an index code.

The complete index codes are collected, and it is calculated that the spatial variances. It can be concluded that the data collected by the pixel in an ideal state are obtained, and the error is relatively small when the centroid position is calculated separately. We fully verify the entire pseudo-random code through the above calculation formula, to obtain the subdivision error as shown in Fig. 8, which compares between the errors of the test device in this paper and the results in literature (Yu et al. 2017). Error is recorded at each 15° point. Simultaneously, we have also added a comparison of the error measurement from literature (Sugiyama et al. 2008). The comparison conclusion of the precision is that the test device has a significant improvement over the literature (Sugiyama et al. 2008), but it is almost flat with the literature (Fig. 9) (Yu et al. 2017).

The comprehensively comparison of key features are shown in Table 3. In effect, the sensor of this paper have been fully improved in performance compared with the literature (Sugiyama et al. 2008) in terms of readout speed and resolution, etc. The sensor of linear-array ensures that the fast readout speed is compared with the area-array sensor, and the pixel array maintain the ideal working state through its special shape, which makes the resolution and precision have certain improvement. In contrast to literature (Yu et al. 2017), the innovation of this paper is to present a unique CMOS linear image sensor and

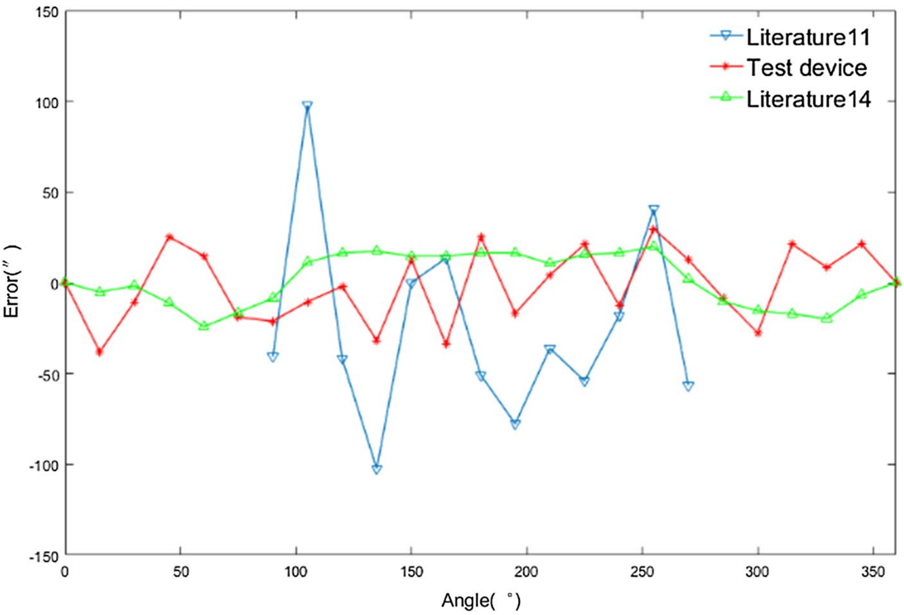

Fig. 9 Measurement error and contrast

Table 3 The comparison of key features

	Literature (Sugiyama et al. 2008)	Literature (Yu et al. 2017)	This paper
Sensor	Area array CMOS	Linear CCD	Linear CMOS
Technology	0.6 µm, 2P3M	/	0.35 µm, 1P3M
Die size	4.0×4.0 mm	/	3.5×1.8 mm
Array size	256×256	640	120
Frame rate	3.2k	/	7.4k
Power dissipation	75 mW@1000 frame/s	/	16 mW@3700 frame/s
Resolution	14 bit	20 bit	20 bit
Deviation of error	50.40″	14.3″	19.41″

to supplement a study on the speed of readout. Likewise, the CMOS sensor scheme has lower power consumption, simple and inexpensive advantages such as comparison with CCD sensor solutions, although it has no advantage in deviation of error.

5 Conclusion

In this paper, a unique CMOS linear image sensor for reading pseudo-random code signal is designed, which has the advantage of matching the pixel array with the slit disc. It effectively reduces the influence of the diffraction phenomenon of light on the detector, and also provides help for the subdivision of pseudo-random code in the aspect of precision. Then we had built a complete test system, and verified that the output signal has good performance in the two aspects of SNR and consistency under the condition of 7.2k frame frequency. The gray-scale centroid method can be used to achieve 20 bit angle resolution.

The research work in this paper verifies the advantages of linear array image sensor combined with pseudo-random code in reading signal speed of image encoder. A unique CMOS linear image sensor is used to collect pseudo-random code, and a better quality analog output signal is obtained. In addition, this method is suitable for low power, simple and inexpensive image encoder systems.

Funding National Key Research and Development Program of China (No. 2017YFF0105303). Technology Development Plan Project of Jilin Province of China (No. 20160204064GX).

References

European Machine Vision Association: EMVA Standard 1288: Standard for Characterization of Image Sensors and Cameras [EB] (2012). http://www.emva.org. October 2018

Feng, Y.Q., Wan, Q.H., Sun, Y., et al.: High resolution interpolation techniques of small photoelectric encoder. Infrared Laser Eng. **42**(7), 1825–1829 (2013)

Jin, J., Zhao, L.N., Xu, S.L.: High-precision rotation angle measurement method based on monocular vision. J. Opt. Soc. Am. A **31**(7), 1401–1407 (2014)

Johnson, J.F., Lomheim, T.S.: Focal-plane signal and noise model–CTIA ROIC. J. IEEE Trans. Electron. Devices **56**(11), 2506–2515 (2009)

Kao, C.F., Huang, H.L., Lu, S.H.: Optical encoder based on Fractional–Talbot effect using two-dimensional phase grating. Opt. Commun. **283**(9), 1950–1955 (2010)

Kim, J.-A., Kim, J.W., Kang, C.-S., Jin, J., Eom, T.B.: Absolute angle measurement using a phase-encoded binary graduated disk. Measurement **80**, 288–293 (2016)

Leviton, D.B., Frey, B.J.: Ultra-high resolution, absolute position sensors for cryostatic applications. Proc. SPIE **4850**, 776–787 (2003)

Luo, W., Zhang, Y., et al.: Pixel super resolution using wavelength scanning. Light Sci. Appl. **5**, e16060 (2016)

Mancini, D., Cascone, E., Schpni, P.: Galileo high-resolution encoder system. Proc. SPIE **3112**, 328–334 (1997)

Pertiu, E.M.: Absolute-type position transducers using a pseudorandom encoding. IEEE Trans. Instrum. Meas. **36**(4), 950–955 (1987)

Qin, J., Silver, R.M., Barnes, B.M., Zhou, H., Dixson, R.G., Henn, M.-A.: Deep subwavelength nanometric image reconstruction using Fourier domain optical normalization. Light Sci. Appl. **5**, e16038 (2016)

Schreier, R., Silva, J.: Design-oriented estimation of thermal noise in switched-capacitor circuits. J. IEEE Trans. Circuits Syst. I Regul. Pap. **52**(11), 2358–2368 (2005)

Sobieranski, A.C., Inci, F., Tekin, H.C., et al.: Portable lensless wide-field microscopy imaging platform based on digital inline holography and multi-frame pixel super-resolution. Light Sci. Appl. **4**, e346 (2015)

Song, P., Ye, Z., Huang, A., et al.: Theoretical investigation on input properties of DI and CTIA readout integrated circuit. J. Opt. Quantum Electron. **48**(3), 185–192 (2016)

Sugiyama, Y., Matsui, Y., et al.: A 3.2 kHz, 14-bit optical absolute rotary encoder with a CMOS profile sensor. IEEE Sens. J. **8**, 1430–1436 (2008)

Tomlinson, G.H.: Elimination of error in absolute position encoder using M-sequences. J. Electron. Lett. **23**(23), 1372–1374 (1987)

Tresanchez, M., Pallejà, T., Teixidó, M., Palacín, J.: Using the image acquisition capabilities of the optical mouse sensor to build an absolute rotary encoder. Sens. Actuators A **157**, 161–167 (2010)

Vermeiren, J., Van Bogget, U., et al.: Low-noise, fast frame-rate In Ga As 320 × 256 FPA for hyperspectral applications. In: Conference on Infrared Technology and Applications XXXV, vol. 7298, p. 72983N. International Society for Optics and Photonics (2009)

Yu, H., Wan, Q.H., et al.: Small-size, high-resolution angular displacement measurement technology based on an imaging detector. Appl. Opt. **56**(3), 755–760 (2017)

Yuan, P., Huang, D., et al.: An anti-spot, high-precision subdivision algorithm for linear CCD based single-track absolute encoder. J. Meas. **37**(03), 143–154 (2019)